



**HAL**  
open science

# **Stark broadening measurements in plasmas produced by laser ablation of hydrogen containing compounds**

Miloš Burger, Jorg Hermann

## **► To cite this version:**

Miloš Burger, Jorg Hermann. Stark broadening measurements in plasmas produced by laser ablation of hydrogen containing compounds. *Spectrochimica Acta Part B: Atomic Spectroscopy*, 2016, 122, pp.118-126. <10.1016/j.sab.2016.06.005>. <hal-02348424>

**HAL Id: hal-02348424**

**<https://hal.science/hal-02348424v1>**

Submitted on 5 Nov 2019

HAL is a multi-disciplinary open access archive for the deposit and dissemination of scientific research documents, whether they are published or not. The documents may come from teaching and research institutions in France or abroad, or from public or private research centers.

L'archive ouverte pluridisciplinaire HAL, est destinée au dépôt et à la diffusion de documents scientifiques de niveau recherche, publiés ou non, émanant des établissements d'enseignement et de recherche français ou étrangers, des laboratoires publics ou privés.



HAL Authorization

# Stark broadening measurements in plasmas produced by laser ablation of hydrogen containing compounds

Miloš Burger<sup>a,\*</sup>, Jörg Hermann<sup>b</sup>

<sup>a</sup>University of Belgrade, Faculty of Physics, POB 44, 11000 Belgrade, Serbia

<sup>b</sup>LP3, CNRS - Aix-Marseille University, 13008 Marseille, France

---

## Abstract

We present a method for the measurement of Stark broadening parameters of atomic and ionic spectral lines based on laser ablation of hydrogen containing compounds. Therefore, plume emission spectra, recorded with an echelle spectrometer coupled to a gated detector, were compared to the spectral radiance of a plasma in local thermal equilibrium. Producing material ablation with ultraviolet nanosecond laser pulses in argon at near atmospheric pressure, the recordings take advantage of the spatially uniform distributions of electron density and temperature within the ablated vapor. By changing the delay between laser pulse and detector gate, the electron density could be varied by more than two orders of magnitude while the temperature was altered in the range from 6,000 to 14,000 K. The Stark broadening parameters of transitions were derived from their simultaneous observation with the hydrogen Balmer alpha line. In addition, assuming a linear increase of Stark widths and shifts with electron density for non-hydrogenic lines, our measurements indicate a change of the Stark broadening-dependence of  $H_\alpha$  over the considered electron density range. The presented results obtained for hydrated calcium sulfate ( $\text{CaSO}_4 \cdot 2\text{H}_2\text{O}$ ) can be extended to any kind of hydrogen containing compounds.

**Keywords:** Stark broadening; Spectra simulation; Hydrogen; Calcium; LIBS.

---

## 1. Introduction

Stark broadening of spectral lines is under investigation since the discovery of the effect in 1913. With the diversification of the available plasma sources and the increasing interest for plasma diagnostic tools, the theoretical and experimental studies dedicated to Stark broadening became popular in the 1960's [1, 2]. Since that time, several review papers have been published to summarize the results obtained by a large number of research groups all over the world [3–7]. Despite of the numerous efforts in the past decades, precise Stark broadening parameters are still only partially available, even for the most prominent transitions. This is mainly due to the difficulties of calibrating the Stark broadening measurements using an alternative and independent measurement method. Recently, Thomson scattering was applied to measure electron density and temperature in laser-produced plasmas [8, 9]. However, the application of this method to high-density thermal plasmas

is doubtful due to electron heating by the probe laser radiation. From the theoretical point of view, there does not exist any model that enables accurate calculations of Stark broadening over a large electron density range, as illustrated by Griem for  $H_\alpha$  [10].

The lack of accurate Stark broadening data and the need of further developments in appropriate models motivate the related research in different types of plasmas. With respect to arcs, sparks or other electrical discharges, the plasmas produced by pulsed lasers are historically younger. This is mainly due to the technological development of laser sources: reliable pulsed lasers that generate highly reproducible plasmas are available since the last two decades only. In addition, the small size and the fast expansion dynamics present particular difficulties for plasma diagnostics. With the invention of gated detectors and the development of applications such as laser-induced breakdown spectroscopy (LIBS), the investigation of plasmas produced by pulsed laser ablation stimulated a strongly growing interest in the past years. The small size and the large initial density now appear as advantages, since the former property limits the optical thickness of plasma emission, and the latter

---

\*Corresponding author: milosb@ff.bg.ac.rs

43 feature favors the establishment of local thermal equi- 95  
44 librium [11, 12]. 96

45 The expansion dynamics of plasmas produced by laser 97  
46 ablation strongly depend on the irradiation conditions 98  
47 and the surrounding atmosphere. The use of infrared 99  
48 radiation favors the absorption of laser photons by the  
49 background gas, leading to an elongated shape of the  
50 plasma [13]. This condition enables rapid intermixing 100  
51 of the ablated vapor with the surrounding atmosphere  
52 [14]. Contrarily, the use of shorter wavelength radia- 101  
53 tion increases the laser-material energy coupling. The  
54 plasma screening effect [15, 16] is reduced, and the 102  
55 plasma is characterized by a hemispherical shape [17]. 103  
56 If, in addition to the use of the short laser wavelength, 104  
57 the ablation process occurs in an argon atmosphere, the 105  
58 ablation plume appears spatially almost uniform. This 106  
59 was illustrated by the analysis of the spectral shapes 107  
60 of resonance lines and strongly Stark-shifted transitions 108  
61 [18]. 109

62 Stark broadening parameters of calcium lines are of in- 110  
63 terest to laboratory plasma diagnostics, as well as for 111  
64 theoretical modeling. In LIBS plasmas for example, 112  
65 Ca is often present as an impurity. Also, due to its 113  
66 large abundance all over the universe, calcium presents 114  
67 a constituent of many stellar plasmas, and Ca and Ca<sup>+</sup> 115  
68 lines are of a great importance in astrophysics [19]. 116  
69 The most intense lines and in particular the ionic res- 117  
70 onance lines were investigated extensively in the past 118  
71 [20–31]. The resonance lines are generally strongly  
72 self-absorbed, and their practical usage for plasma diag- 119  
73 nostics is often doubtful. Stark broadening calculations, 120  
74 based on the semiclassical perturbation formalism, have  
75 been performed for many Ca [19, 32] and Ca<sup>+</sup> transi- 121  
76 tions [33, 34]. The correlation of Stark broadening with  
77 the energy gap between the upper-level of the transition  
78 and the ionization potential was also investigated [35]. 122  
79 However, Stark parameters of many Ca transitions in the  
80 visible and UV ranges are still missing in literature. 123

81 In the present work, we take advantage of the spa- 124  
82 tially uniform character of the plasma produced by UV 125  
83 nanosecond laser ablation in argon at near atmospheric 126  
84 pressure. Samples of hydrated calcium sulfate were ab- 127  
85 lated to obtain spectral line emission from hydrogen, 128  
86 calcium, oxygen and several impurities. Comparing 129  
87 the measured emission spectrum to the spectral radi- 130  
88 ance computed for a uniform plasma in local thermo-  
89 dynamic equilibrium, we were able to characterize the 131  
90 plasma and to deduce the Stark broadening parameters  
91 for many atomic and ionic lines. With respect to the tra- 132  
92 ditional methods based on space-resolved spectroscopic  
93 measurements and complex data analysis via Abel in-  
94 version [20, 28, 36], the presented method appears eas-

ier to handle and gives rapid access to a large number  
of data. Indeed, using an echelle spectrometer of large  
resolving power, the recording of a few spectra at dif-  
ferent delays enables the determination of Stark broad-  
ening parameters of a large number of spectral lines.

## 100 2. Method and calculation details

### 101 2.1. Principle of Stark broadening measurements

102 The method for the measurement of Stark broaden-  
103 ing parameters consists of the following three succes-  
104 sive steps: (i) the plasma temperature  $T$ , the electron  
105 density  $n_e$ , and the relative fractions of elements  $C$  were  
106 deduced for spectra recorded at different times (delay  
107 between laser pulse and detector gate) using the itera-  
108 tive procedure decribed in Ref. [37]. Here,  $n_e$  is de-  
109 duced from  $H_\alpha$  for which accurate electron density mea-  
110 surements are expected for  $n_e$ -values of the order of  
111  $10^{17} \text{ cm}^{-3}$  [10]; (ii) Once the plasma is characterized,  
112 the Stark widths and shifts of non-hydrogenic lines are  
113 deduced from best agreement between measured and  
114 computed spectra. The plasma being characterized pre-  
115 viously, the calculation of the line profiles accounts  
116 for Doppler- and resonance broadening; (iii) The Stark  
117 broadening parameters  $w$  and  $d$  of the non-hydrogenic  
118 lines were deduced from the linear increase of Stark  
119 width and shift with  $n_e$ .

### 120 2.2. Calculation details

121 Material ablation with pulsed lasers in a background  
122 gas at near atmospheric pressure leads to almost hemi-  
123 spherical expansion if the interaction of the laser beam  
124 with the gas is negligible, and the laser spot diameter is  
125 small compared to the plasma radius. In that case, the  
126 blast wave model may be applied to describe the plume  
127 expansion dynamics. The conditions are fulfilled for ul-  
128 traviolet nanosecond laser pulses [13, 17]. If argon is  
129 used as a buffer gas, the spatial distributions of electron  
130 density and temperature within the ablated vapor are al-  
131 most uniform and the spectral radiance of the plasma  
132 can be calculated using [37]

$$133 I_\lambda = U_\lambda(1 - e^{-\alpha L}), \quad (1)$$

134 where  $U_\lambda$  is the black-body spectral radiance,  $L$  is the  
135 plasma diameter along the observation direction, and  $\alpha$   
136 is the absorption coefficient given by [1]

$$137 \alpha(\lambda) = \pi r_0 \lambda^2 f_{lu} n_l P(\lambda) (1 - e^{-hc/\lambda kT}). \quad (2)$$

138 Here,  $r_0$  is the classical electron radius,  $\lambda$  is the wave-  
139 length,  $h$  is the Planck constant,  $c$  is the vacuum light

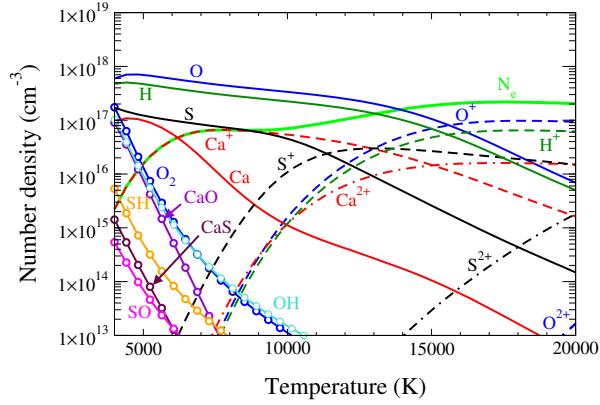


Figure 1: Number densities of species versus temperature computed for a  $\text{CaSO}_4 \cdot 2\text{H}_2\text{O}$  plasma in LTE at atmospheric pressure.

velocity,  $k$  is the Boltzmann constant,  $f_{lu}$  and  $n_l$  are the absorption oscillator strength and the lower level population number density of the transition, respectively. The normalized line profile  $P(\lambda)$  is calculated considering Doppler and Stark broadening that are the dominant mechanisms of spectral line broadening in strongly ionized laser-produced plasmas [38]. Depending on the relative values of Doppler and Stark widths, the line shapes are described by Gaussian, Lorentzian or Voigt profiles. The Doppler width is calculated according to plasma temperature and atomic mass of the emitting species. The Stark width is obtained using [10, 39]

$$\Delta\lambda_{\text{Stark}} = w \left( \frac{n_e}{n_e^{\text{ref}}} \right)^m, \quad (3)$$

where  $w$  is the Stark width at the reference electron density  $n_e^{\text{ref}}$ . The Stark shift is obtained from Eq. (3) replacing  $w$  by the Stark shift at the reference electron density  $d$ . We assumed linear dependence of Stark width with electron density ( $m = 1$ ) for all non-hydrogenic lines. For the  $\text{H}_\alpha$  transition, different  $m$ -values were reported in literature. The values obtained from theory vary from 0.68 to 0.83 whereas  $m \approx 0.35$  was reported for experiments [10]. In the present work, we use for  $n_e \leq 1 \times 10^{17} \text{ cm}^{-3}$  the expression proposed by Gigoso et al. [40], using Eq. (3) with  $w = 1.10 \text{ nm}$ ,  $n_e^{\text{ref}} = 1 \times 10^{17} \text{ cm}^{-3}$ , and  $m = 0.68$ . For larger electron densities, we use a slightly different expression with a somewhat larger experimentally determined  $m$ -value (see section 4.2). We stress that Stark broadening of  $\text{H}_\alpha$  is recognized as a reliable tool for  $n_e$ -measurements in laser-induced plasmas [41].

The lower level population number density in Eq. (2) is obtained by calculating the plasma composition assuming local thermodynamic equilibrium (LTE) [42]. The

number densities of plasma species computed for LTE are displayed in Fig. 1 for the elemental composition of the here investigated hydrated calcium sulfate sample. The calculations have been performed by setting the kinetic pressure of the plasma to atmospheric pressure [42]. As the pressure is kept constant, the atomic number densities of elements and thus the total atomic number density of the plasma decrease with increasing temperature.

In the considered temperature range, atomic and ionic species dominate the plasma composition. Molecular species significantly contribute to the plasma composition only for  $T < 5,000 \text{ K}$ . According to the moderate dissociation energies of the involved diatomic species [43], their number densities decrease rapidly with temperature, representing a fraction  $< 1\%$  for  $T = 6,000 \text{ K}$ . For  $T \leq 15,000 \text{ K}$ , neutral atoms are the dominating plasma species according to the large ionization potentials of the most abundant elements H and O [44]. The ionization potential of Ca being of only 6 eV, the electrons originate essentially from the ionization of calcium in the temperature range up to 9,000 K. For  $T > 9,000 \text{ K}$ , the ionization of sulfur contributes significantly to the plasma ionization whereas  $T > 12,000 \text{ K}$  is required to enable strong contributions of oxygen and hydrogen. The temperature dependence of the  $\text{Ca}^{2+}$  number density is similar to those of  $\text{O}^+$  and  $\text{H}^+$ . This is due to the ionization potential of  $\text{Ca}^+$  that is close to the ionization energies of O and H. For  $T > 15,000 \text{ K}$ , the ionic species dominate the plasma and  $\text{O}^+$  and  $\text{H}^+$  ions are the most abundant species.

### 3. Experiment

The experiments were carried out with a frequency-quadrupled Nd:YAG laser (Quantel, model Brilliant) delivering pulses of 4 ns duration and 40 mJ energy at the wavelength of 266 nm. The laser pulse energy was attenuated to 6 mJ by turning the beam polarization with the aid of a half-wave plate and crossing through a polarization analyzer. The laser beam was focused onto the sample surface using a plano-convex lens of 150 mm focal length. According to a spot diameter of  $100 \mu\text{m}$  of the Gaussian beam, a laser fluence of about  $80 \text{ J cm}^{-2}$  was obtained on the sample surface. The pellet samples were prepared from commercially available hydrated calcium sulfate powder using a hydraulic press, and placed on a motorized sample holder in a vacuum chamber of  $10^{-4} \text{ Pa}$  residual pressure. During the experiments, the chamber was filled with argon at  $5 \times 10^4 \text{ Pa}$  pressure. The plasma emission was captured by imaging the plume with two lenses of 150 and 35

223 mm focal lengths onto the entrance of an optical fiber  
 224 of 600  $\mu\text{m}$  diameter. The optical axis of the lenses was  
 225 tilted by  $15^\circ$  with respect to the surface normal. Accord-  
 226 ing to the image magnification of about 1.5, a cylindri-  
 227 cal volume of about 3 mm diameter was observed. The  
 228 fiber was coupled to the entrance of an echelle spec-  
 229 trometer (LTB, model Aryelle Butterfly) of 0.4 m focal  
 230 length and a resolving power of  $8.9 \times 10^3$ . Photon de-  
 231 tection was ensured using an intensified charge-coupled  
 232 device matrix detector (Andor, model IStar). The spec-  
 233 tral resolution of the apparatus was measured using a  
 234 low-pressure argon-mercury lamp. An intensity calibra-  
 235 tion of the spectroscopic apparatus was performed in the  
 236 visible and UV spectral ranges using a calibrated tung-  
 237 sten lamp (Oriel, model 63358) and a deuterium lamp  
 238 (Heraeus, model DO544J), respectively.  
 239 The spectra were recorded for different delays of the de-  
 240 tector gate  $t_g$  with respect to the laser pulse. The gate  
 241 width  $\Delta t_g$  was adjusted for each delay so that  $\Delta t_g < t_g$ .  
 242 We denote the measurement time  $t = t_g \pm \Delta t_g/2$ . To  
 243 enhance the signal-to-noise ratio, data acquisition was  
 244 performed by averaging over 500 ablation events, ap-  
 245 plying 5 pulses to 100 different irradiation sites. The  
 246 sites were separated by a distance of 150  $\mu\text{m}$ .

247 **4. Results and discussion**

248 **4.1. Plasma characterization**

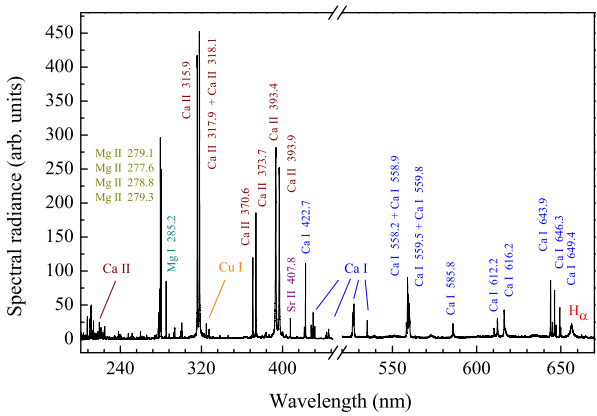


Figure 2: Spectrum recorded during ablation of hydrated calcium sulfate for  $t = (475 \pm 75)$  ns.

249 The emission spectrum of the plasma produced by  
 250 laser ablation of hydrated calcium sulfate is displayed  
 251 in Fig. 2 for the spectral ranges that exhibit the most  
 252 significant investigated transitions. To facilitate the  
 253 observation of the low-intensity transitions in the green-  
 254 red range, the intensity scale was multiplied by a factor

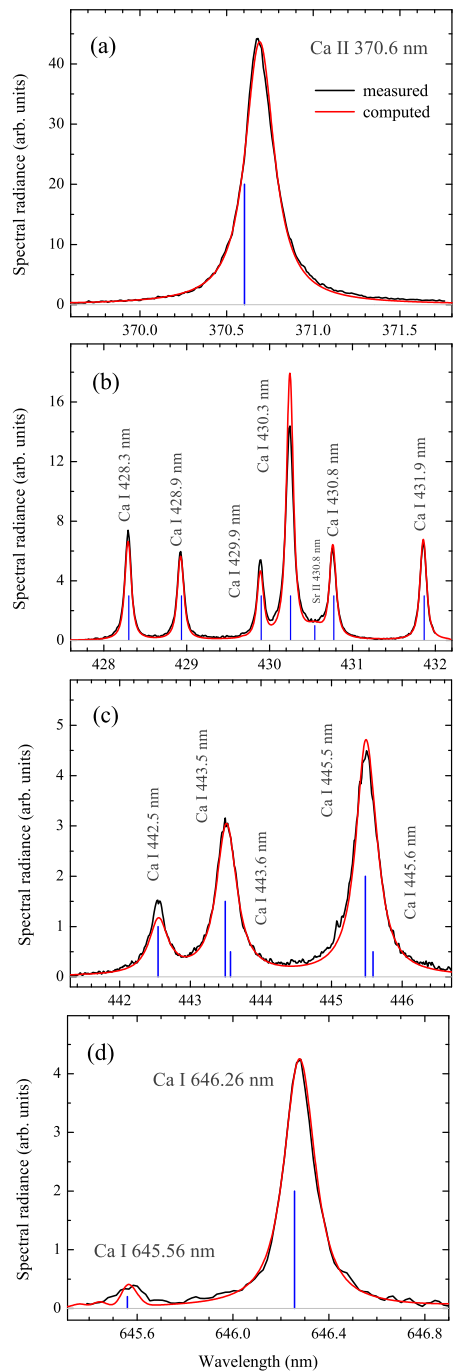


Figure 3: Measured spectrum (black line) and computed spectral radiance (red line) of various calcium transitions. The computed radiance was obtained for  $T = 12,200$  K,  $n_e = 1.6 \times 10^{17}$   $\text{cm}^{-3}$ ,  $L = 0.65$  mm and the elemental composition given in Table 1. The blue lines denote the resonance wavelength of each transition.

of 10 for that part of the spectrum. The plasma emission is dominated by spectral lines of singly charged calcium ions. In addition, transitions of Ca neutral atoms and of species from several impurity elements are observed. We identify the strongly broadened  $H_\alpha$  transition in the red range of the spectrum. The atomic fractions of both major and minor elements deduced from the best agreement between measured and computed spectra are given in Table 1.

The spectrum measured for  $t = (475 \pm 75)$  ns (see Fig. 2) is displayed in Fig. 3 for several spectral ranges, together with the computed spectral radiance. We observe a good agreement between measured and computed spectral shapes for all presented transitions. It is shown that the lines are significantly broadened. Some transitions such as Ca II 370.6 nm (a) and Ca I 646.26 nm (d) are characterized by large Stark shifts. A slight difference in intensity is visible for some lines and in particular for Ca I 430.3 nm. The mismatch is attributed to the low accuracy of the transition probabilities [44]. The time-evolution of the laser-induced plasma was investigated by recording spectra for different observation delays with respect to the laser pulse. The characteristic behavior is illustrated in Fig. 4 where the spectral shapes of  $H_\alpha$  (a), Ca I 585.74 nm (b), and Mg I 285.21 nm (c) are shown for different times. We observe strong broadening at early times followed by consecutive narrowing of the line profiles with increasing time. In addition, Ca I 585.74 nm and Mg I 285.21 nm exhibit large red-shifting at early times. Transitions of large Stark shift are characterized by asymmetric line shapes if they are emitted from a spatially non-uniform plasma [18]. Here, the symmetric shape observed for the Mg I 285.21 nm line (c) shows that the plasma is spatially uniform in agreement with

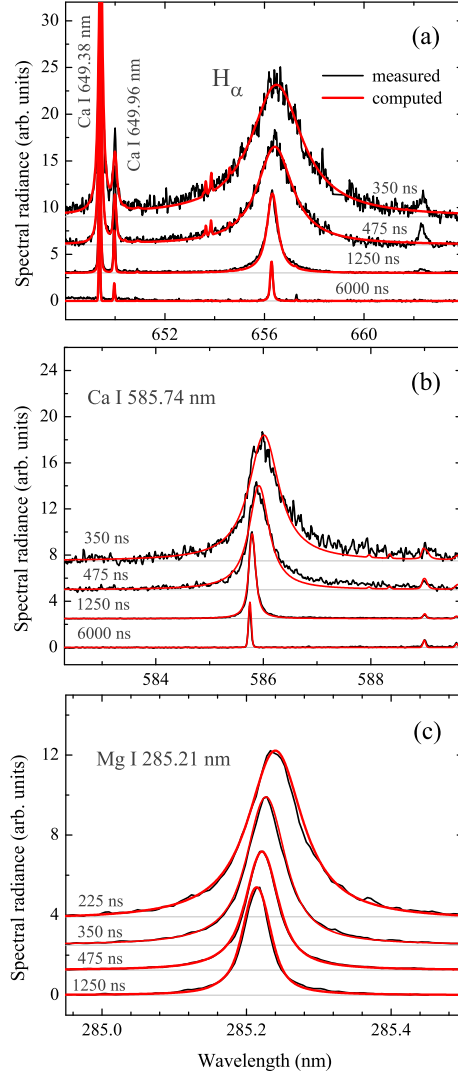


Figure 4: Measured (black line) and computed (red line) spectral radiance of several transitions for different observation times.

Table 1: Atomic fractions of the constituents of the hydrated calcium sulphate pellet deduced from the LIBS spectra  $C_{LIBS}$ . The reference values  $C_{ref}$  correspond to the chemical formula  $CaSO_4 \cdot 2H_2O$ .

Elmnt.	$C_{LIBS}(\%)$	$C_{ref}(\%)$
Ca	9.1	8.3
S	8.3	8.3
O	47	50.0
H	35	33.3
Cu	0.04	-
Fe	0.014	-
Li	0.017	-
Mg	0.4	-
Si	0.08	-
Sr	0.012	-

previous observations of LIBS plasmas produced in argon background gas [37, 45].

The plasma temperature evolution is illustrated by the Saha-Boltzmann plots displayed in Fig. 5. Here,  $\epsilon$  is the emission coefficient deduced from the measurements using  $\epsilon = \epsilon_c I_m / I_c$ , where  $\epsilon_c$  is the calculated emission coefficient, and  $I_m$  and  $I_c$  are the measured and computed line-integrated spectral radiances, respectively. As the computed radiance intrinsically accounts for self-absorption, the Saha-Boltzmann plot displayed in Fig. 5 is equivalent to the Boltzmann plot corrected for self-absorption presented by Bulajic et al. [46]. It is

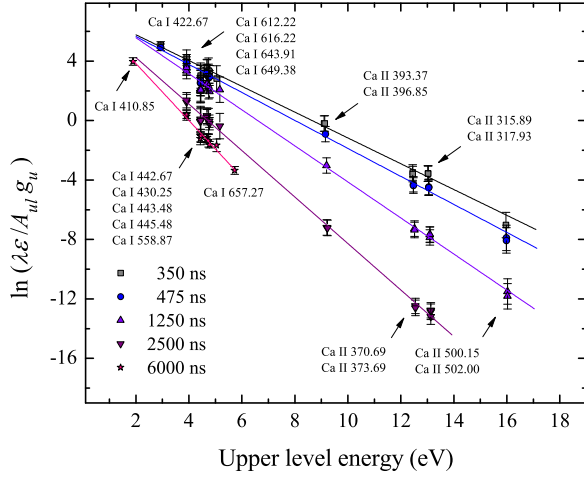


Figure 5: Saha-Boltzmann plots of calcium for various observation times.

shown that the population number densities of atomic and ionic excited species are well described by the equilibrium distribution for all measurement times.

The deduced values of temperature and electron density are shown in Fig. 6 as functions of time. The horizontal error bars represent the gate width, whereas the vertical error bars stand for the measurement uncertainties. According to Griem [10], electron density measurements using  $H_\alpha$  are most precise for  $n_e$ -values close to  $10^{17} \text{ cm}^{-3}$ . The measurement error increases with distance from that value due to the uncertainty of the exponent  $m$  (see Eq. 3). We estimated the  $n_e$ -measurement error assuming uncertainties of 10% for the parameters  $w$  and  $m$  and of 5% for the Stark width measurement. During the considered time-interval from 200 to 6000 ns, the electron density decreases by more than two orders of magnitude from  $5 \times 10^{17}$  to  $3 \times 10^{15} \text{ cm}^{-3}$ , whereas the temperature diminishes from about 14,000 to 6,000 K.

#### 4.2. Stark width and shift measurements

The strong variation of electron density over the measured time-interval and the spatially uniform character of the laser-produced plasma are now explored to measure the Stark widths and shifts of spectral lines. We emphasize that the calculation of the spectral radiance allows us to predict the optical thickness of each transition, and thus to exclude strongly self-absorbed lines from the analysis. For some transitions such as resonance lines of neutral atoms, the optical thickness critically depends on the observation delay. At early time, when the plasma temperature is high and ionic species

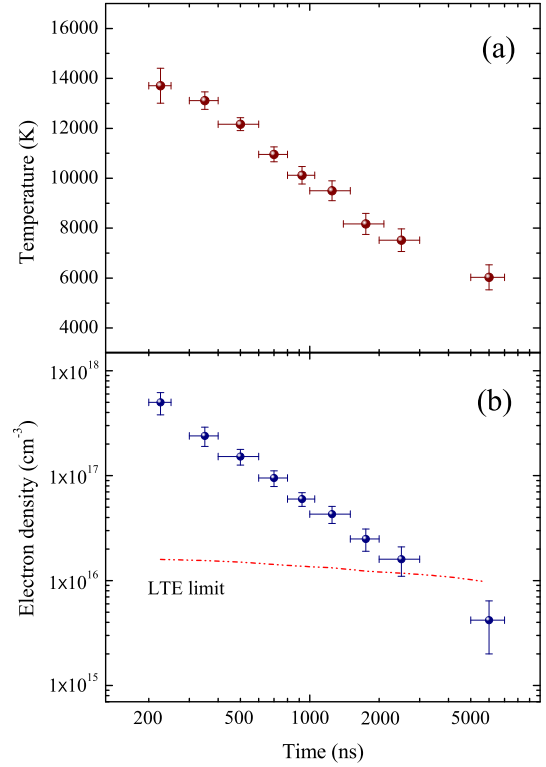


Figure 6: Temporal evolution of electron density (a) and excitation temperature (b). The dashed red line (b) stands for the minimum  $n_e$ -value required for LTE according to the McWhirter criterion [47].

dominate (see Fig. 1), the ground state population number densities of neutral atoms are small and their resonance lines have little optical thickness. Contrarily, at late times, when the temperature is low, neutral atoms dominate, their ground state population number densities are large, and self-absorption of resonance lines is strong.

For transitions of large Stark shift, the influence of the optical thickness on the spectral line shape can be verified by analyzing the correlation between Stark width and shift. This is illustrated in Fig. 7, where the linear increase of Stark shift with Stark width is observed for transitions of Ca and  $\text{Ca}^+$ .

The spectral lines having small optical thickness over the entire time-interval were used to analyse the dependence of their Stark widths and shifts on the Stark width of the  $H_\alpha$  transition. This is shown in Fig. 8 where the Stark width of Ca I 585.74 nm is presented versus  $H_\alpha$  Stark width on a logarithmic scale. Assuming linear dependencies of Stark width with electron density for non-hydrogenic transitions, we can deduce from the slope the exponent  $m$  that characterizes the dependence of the  $H_\alpha$  Stark width on  $n_e$  (see Eq. 3). We observe in

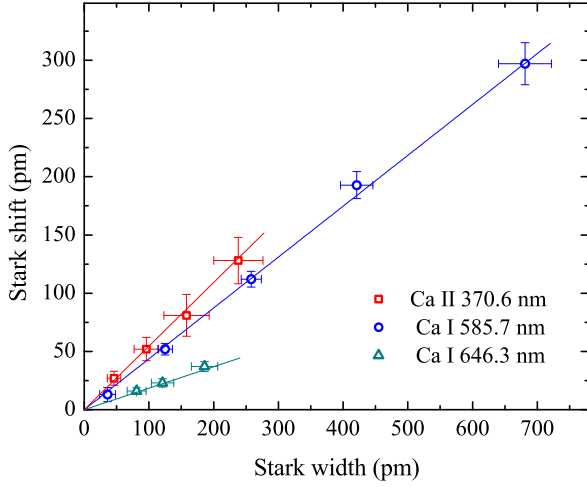


Figure 7: Stark shift vs Stark width of calcium lines deduced from measurements at various delays.

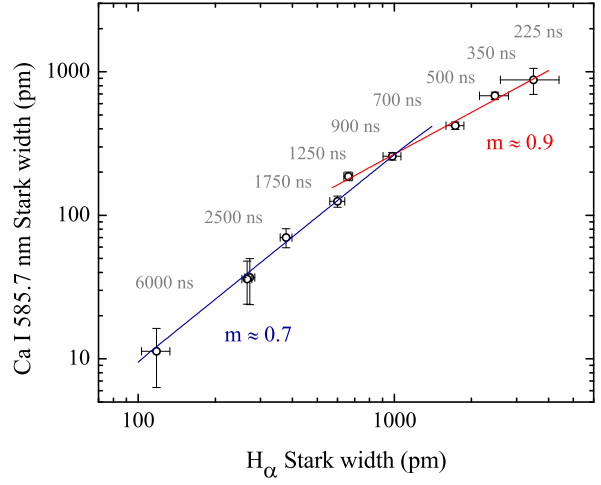


Figure 8: Stark width of a non-hydrogenic transition vs  $H_\alpha$  Stark width. We deduce slightly different  $m$ -values for  $H_\alpha$  Stark broadening (see Eq. 3) for the  $n_e$ -ranges below and above  $1 \times 10^{17} \text{ cm}^{-3}$ .

357 Fig. 8 two slightly different slopes, indicating that the  
 358  $n_e$ -dependence of  $H_\alpha$  Stark broadening in the low elec-  
 359 tron density range differs from that at large  $n_e$ -values.  
 360 The transition between both regimes corresponds to a  
 361 delay  $\approx 1000$  ns for which the electron density is close  
 362 to  $1 \times 10^{17} \text{ cm}^{-3}$ . We thus describe Stark broadening  
 363 of  $H_\alpha$  using Eq. (3) with  $w = 1.10$  nm according to liter-  
 364 ature [40, 48] and  $m = 0.7$  or  $m = 0.9$  for electron  
 365 densities below or above  $n_e^{ref} = 1 \times 10^{17} \text{ cm}^{-3}$ , respec-  
 366 tively. It is noted that the expression equals that pro-  
 367 posed by Gigosos et al. [40] and Konjevic et al. [48]  
 368 for  $n_e < 1 \times 10^{17} \text{ cm}^{-3}$  whereas it differs at larger elec-  
 369 tron densities by the  $m$ -value exclusively. According to  
 370 the good agreement between measured and computed  
 371 Stark widths for  $n_e \approx 1 \times 10^{17} \text{ cm}^{-3}$  reported in litera-  
 372 ture [10] (see section 2) we estimate the uncertainty to  
 373  $\approx 10\%$  for  $n_e$ -values close to  $n_e^{ref}$ . The error increases  
 374 with distance from the reference electron density due to  
 375 the uncertainty of  $m$ .  
 376

#### 377 4.3. Determination of Stark broadening parameters

378 After the implementation of the electron density  
 379 measurement procedure using  $H_\alpha$ , we explore now  
 380 the linear dependence of Stark widths and shifts on  
 381  $n_e$  for non-hydrogenic transitions to determine their  
 382 Stark broadening parameters  $w$  and  $d$ . Therefore, the  
 383 Stark widths and shifts of non-hydrogenic transitions  
 384 were measured for the spectra recorded with different  
 385 delays and plotted as functions of electron density  
 386 as shown in Fig. 9. According to the precise linear  
 387 increase, the relative errors arising from the linear

388 analysis are small compared to the absolute errors  
 389 associated to the electron density measurement using  
 390  $H_\alpha$ . Thus, for isolated lines of measurable Stark width  
 391 over a large  $n_e$ -range, the errors of the deduced  $w$ - and  
 392  $d$ -values are close to those of the most accurate  $n_e$ -  
 393 measurements, evaluated to about 15%. For transitions  
 394 having measurable Stark width in a restricted  $n_e$ -range  
 395 only, the measurement errors of  $w$  and  $d$  are naturally  
 396 larger.  
 397

398 The deduced broadening parameters are presented in  
 399 Tables 2 and 3 for the spectral lines of calcium and other  
 400 elements, respectively. Assuming an accuracy of elec-  
 401 tron density measurements of about 15% for  $n_e$ -values  
 402 close to  $10^{17} \text{ cm}^{-3}$ , the estimated  $w$ -measurement error  
 403 ranges from 20 to 30% for most transitions. For some  
 404 lines, the accuracy is lower due to larger contributions  
 405 of apparatus- and/or resonance broadening to the line  
 406 profile. Compared to Stark broadening parameters re-  
 407 ported in literature (see last two columns in the Tables),  
 408 a mismatch larger than the estimated accuracy is ob-  
 409 served for several lines. Depending on the multiplet,  
 410 the values reported in literature are larger or smaller  
 411 than the broadening parameters we report here. The  
 412 large dispersion  $w$ - and  $d$ -values measured in different  
 413 experiments is attributed to two main causes: (i) the  
 414 uncertainty of electron density due to the difficulties of  
 415 calibrating the  $n_e$ -measurements. Indeed, absolute val-  
 416 ues of electron density are exclusively obtained through  
 417 the calculation of Stark broadening parameters leading  
 418 to a large variability of  $n_e$  that depends on the chosen

Table 2: Wavelength  $\lambda$ , configuration and term of upper and lower excitation levels of transitions according to NIST [44]. The measured Stark width  $w$  and shift  $d$  and the values reported in literature  $w^{lit}$  and  $d^{lit}$  are given for  $n_e = 1 \times 10^{17} \text{ cm}^{-3}$ .  $\Delta w/w$  and  $\Delta d/d$  are the relative errors of the measured Stark width and shift, respectively.

Species	$\lambda$ (nm)	Lower level Config.	Term	Upper level Config.	Term	$w$ (pm)	$\Delta w/w$ (%)	$d$ (pm)	$\Delta d/d$ (%)	$w^{lit}$ (pm)	$d^{lit}$ (pm)
Ca I	299.496 299.732 300.086 300.686 300.921	$3p^6 4s 4p$	$^3P^o$	$3p^6 3d^2$	$^3P$	23	20	4.4	30	$29^a$	-
Ca I	422.673	$3p^6 4s^2$	$^1S$	$3p^6 4s 4p$	$^1P^o$	32	60	6	40	-	-
Ca I	429.899 430.253 430.774 431.865	$3p^6 4s 4p$	$^3P^o$	$3p^6 4p^2$	$^3P$	40	25	-8	40	-	-
Ca I	442.544 443.496 443.568 445.478 445.589 445.662	$3p^6 4s 4p$	$^3P^o$	$3p^6 4s 4d$	$^3D$	200	20	-	-	$15.5^a$	-
Ca I	558.197 558.875 559.011 559.446 559.848	$3p^6 3d 4s$	$^3D$	$3p^6 3d 4p$	$^3D^o$	90	20	28	30	-	-
Ca I	585.745	$3p^6 4s 4p$	$^1P^o$	$3p^6 4p^2$	$^1D$	260	20	100	20	-	-
Ca I	612.222	$3p^6 4s 4p$	$^3P^o$	$3p^6 4s 5s$	$^3S$	165	20	75	20	-	-
Ca I	643.908 646.257 649.378	$3p^6 3d 4s$	$^3D$	$3p^6 3d 4p$	$^3F^o$	66	20	14	30	-	-
Ca II	210.324 211.276	$3p^6 4p$	$^2P^o$	$3p^6 5d$	$^2D$	104	20	30	20	$67^b$ $73^b$	$23^b$ $26^b$
Ca II	370.602 373.690	$3p^6 4p$	$^2P^o$	$3p^6 5s$	$^2S$	79	25	47	20	$135^d$ $183^d$	$35^c$ $35^c$

<sup>a</sup> Ref. [25], <sup>b</sup> Ref. [31], <sup>c</sup> Ref. [28], <sup>d</sup> Ref. [24].

Table 3: Wavelength  $\lambda$ , configuration and term of upper and lower excitation levels of transitions according to NIST [44]. The measured Stark width  $w$  and shift  $d$  and the values reported in literature  $w^{lit}$  and  $d^{lit}$  are given for  $n_e = 1 \times 10^{17} \text{ cm}^{-3}$ .  $\Delta w/w$  and  $\Delta d/d$  are the relative errors of the measured Stark width and shift, respectively.

Species	$\lambda$ (nm)	Lower level Config.	Term	Upper level Config.	Term	$w$ (pm)	$\Delta w/w$ (%)	$d$ (pm)	$\Delta d/d$ (%)	$w^{lit}$ (pm)	$d^{lit}$ (pm)
C I	247.856	$2s^2 2p^2$	$^1S$	$3s^2 2p 3s$	$^3P^o$	14	30	8	25	$6.8^e$	$2.6^e$
Cu II	212.604	$3d^9(^2D)4s$	$^3D$	$3d^9(^2D)4p$	$^3F^o$	6	30	1.1	50	$8.2^f$	-
Mg I	213.598										
Mg I	277.669	$3s 3p$	$^3P^o$	$3p^2$	$^3P$	7	40	1	100	-	-
Mg I	277.827										
Mg I	278.141										
Mg I	278.297										
Mg I	285.212	$2p^6 3s^2$	$^1S$	$3s 3p$	$^1P^o$	17	30	8.5	30	-	-
Mg I	382.935	$3s 3p$	$^3P^o$	$3s 3d$	$^3D$	270	20	-45	30	$110^g$	$-2^g$
Mg I	383.230										
Mg I	383.829										
Mg I	516.732	$3s 3p$	$^1P^o$	$3s 4s$	$^3S$	90	20	50	20	$33^g$	$9^g$
Mg I	517.268									$35.5^g$	$8.4^g$
Mg I	518.360									$35^g$	$7.4^g$
Mg II	279.077	$2p^6 3p$	$^2P^o$	$2p^6 3d$	$^2D$	30	20	9	25	$162^h$	$22^h$
Mg II	279.799									$144^h$	$19^h$
Mg II	292.863	$2p^6 3p$	$^2P^o$	$2p^6 4s$	$^2S$	50	20	23	20	$29^i$	$57^i$
Mg II	293.651									$30^i$	$68^i$
Si I	250.689	$3s^2 3p^2$	$^3P$	$3s^2 3p 4s$	$^3P^o$	14	25	8	25	$14.1^j$	-
Si I	251.431									$11.2^j$	
Si I	251.611									$11.7^j$	
Si I	251.920									$11.2^j$	
Si I	252.410									$10.4^j$	
Si I	252.850									$10.7^j$	
Fe II	238.203	$3d^6(^5D)4s$	$a^6D$	$3d^6(^5D)4p$	$z^6F^o$	5	30	2	30	-	-
Fe II	238.862										
Fe II	239.562										
Fe II	239.924										
Fe II	240.488										
Fe II	241.051										
Fe II	259.587	$3d^6(^5D)4s$	$a^6D$	$3d^6(^5D)4p$	$z^6D^o$	6	30	0.8	60	-	-
Fe II	259.836										
Fe II	259.939									$4.5^k$	-
Fe II	260.708										
Fe II	261.187										
Fe II	261.382										
Fe II	273.954	$3d^6(^5D)4s$	$a^4D$	$3d^6(^5D)4p$	$z^4D^o$	9	30	3	35	$5.3^l$	-
O I	777.194	$2s^2 2p^3(^4S^o)3s$	$^5S^o$	$2s^2 2p^3(^4S^o)3p$	$^5P$	105	35	15	40	-	-
O I	777.416										
O I	777.538										
Sr II	407.770	$4p^6 5s$	$^2S$	$4p^6 5p$	$^2P^o$	41	20	-3.4	30	-	-
Sr II	421.551										

<sup>e</sup> Ref. [49], <sup>f</sup> Ref. [50], <sup>g</sup> Ref. [51], <sup>h</sup> Ref. [52], <sup>i</sup> Ref. [53], <sup>j</sup> Ref. [54], <sup>k</sup> Ref. [55], <sup>l</sup> Ref. [56].

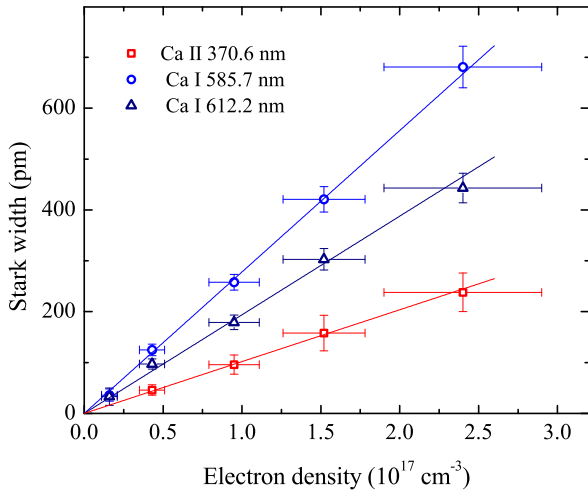


Figure 9: Stark widths of Ca I and Ca II transitions vs electron density.

419 transition and the  $n_e$ -range. (ii) The measurements re-  
 420 ported in literature were performed using various types  
 421 of plasmas characterized by different temperatures. Al-  
 422 though the  $T$ -dependence was neglected in the present  
 423 work according to the moderate temperature variation in  
 424 the laser-produced plasma, the changes of Stark broad-  
 425 ening parameters with temperature cannot be neglected  
 426 in case of strong  $T$ -variation.  
 427 As an example, the large variability of Stark broadening  
 428 parameters in literature is illustrated by the  $w$ -values of  
 429 6.8 and 54 pm reported for C I 247.85 nm [3, 49]. We  
 430 stress that the most intense spectral lines (see Fig. 2)  
 431 were not considered as their large optical thickness pre-  
 432 vent the accurate Stark width measurement.

## 433 5. Conclusion

434 We presented a method for the measurement of Stark  
 435 broadening parameters based on modeling of the emis-  
 436 sion spectrum from a laser-induced plasma. Produc-  
 437 ing ablation with ultraviolet nanosecond laser pulses in  
 438 argon at near atmospheric pressure, the measurements  
 439 take advantage of the spatially uniform distributions of  
 440 electron density and temperature within the ablated va-  
 441 por plume. These properties enable simple and accurate  
 442 modeling based on the calculation of the spectral radi-  
 443 ance of a plasma in local thermodynamic equilibrium.  
 444 The spectra recording with an echelle spectrometer of  
 445 large resolving power give access to analysis of a large  
 446 number of spectral lines. Using hydrated calcium sul-  
 447 phate as sample material, we were able to deduce the  
 448 Stark broadening parameters of atomic and ionic spec-  
 449 tral lines from calcium, oxygen and several impurity el-

450 ements by their simultaneous observation with the  $H_\alpha$   
 451 transition. By varying the delay of the detector gate with  
 452 respect to the laser pulse, the electron density was varied  
 453 by more than two orders of magnitude from  $3 \times 10^{15}$   
 454 to  $5 \times 10^{17} \text{ cm}^{-3}$  whereas temperature was changed  
 455 from about 6,000 to 14,000 K. Assuming a linear in-  
 456 crease of Stark widths of non-hydrogenic lines with  $n_e$ ,  
 457 the present analysis indicate a change of the  $H_\alpha$  Stark  
 458 width-dependence on  $n_e$  that occurs when the electron  
 459 density varies from values  $< 10^{17} \text{ cm}^{-3}$  to larger density.  
 460 For  $n_e > 10^{17} \text{ cm}^{-3}$ , we observe a more *non-hydrogenic*  
 461 behaviour whereas the typical  $n_e^{2/3}$ -dependence was re-  
 462 trieved for the low electron density range, in agreement  
 463 with theoretical predictions. According to the precise  
 464 electron density measurements for  $n_e$ -values close to  
 465  $1 \times 10^{17} \text{ cm}^{-3}$ , the deduced Stark broadening param-  
 466 eters have fair uncertainties of 20 to 30% for most of the  
 467 investigated transitions.

## 468 6. Acknowledgements

469 The authors acknowledge the financial support  
 470 provided by LASERLAB- EUROPE (grant agreement  
 471 No. 284464, project CNRS-LP3002148). This research  
 472 has also been supported by the Ministry of education,  
 473 science and technological development of the Republic  
 474 of Serbia (project ON171008).

- 475 [1] H. R. Griem, Plasma spectroscopy, Academic Press, New York,  
 476 1964.
- 477 [2] H. R. Griem, Spectral line broadening of plasmas, Academic  
 478 Press, New York, 1974.
- 479 [3] N. Konjević, J. R. Roberts, A critical review of the Stark widths  
 480 and shifts of spectral lines from non-hydrogenic atoms, J. Phys.  
 481 Chem. Ref. Data 5 (1976) 209–257.
- 482 [4] N. Konjević, M. S. Dimitrijević, W. L. Wiese, Experimental  
 483 Stark widths and shifts for spectral lines of neutral atoms (A  
 484 critical review of selected data for the period 1976 to 1982), J.  
 485 Phys. Chem. Ref. Data 13 (1984) 619–647.
- 486 [5] N. Konjević, A. Lesage, J. R. Führ, W. L. Wiese, Experimental  
 487 Stark widths and shifts for spectral lines of neutral and ionized  
 488 atoms (A critical review of selected data for the period 1983  
 489 through 1988), J. Phys. Chem. Ref. Data 19 (1990) 1307–1385.
- 490 [6] N. Konjević, A. Lesage, J. R. Führ, W. L. Wiese, Experimental  
 491 Stark widths and shifts for spectral lines of neutral and ionized  
 492 atoms (A critical review of selected data for the period 1989  
 493 through 2000), J. Phys. Chem. Ref. Data 31 (2002) 819–921.
- 494 [7] A. Lesage, Experimental Stark widths and shifts for spectral  
 495 lines of neutral and ionized atoms A critical review of selected  
 496 data for the period 2001–2007, N. Astron. Rev. 52 (2009) 471–  
 497 535.
- 498 [8] A. Mendys, K. Dzierżęga, M. Grabiec, S. Pellerin, B. P. G., Tra-  
 499 vaillé, B. Bousquet, Investigations of laser-induced plasma in  
 500 argon by thomson scattering, Spectrochim. Acta Part B: Atom.  
 501 Spectrosc. 66 (2011) 691–697.
- 502 [9] M. Cvejić, K. Dzierżęga, T. Pięta, Investigation of thermody-  
 503 namic equilibrium in laser-induced aluminum plasma using the  
 504

- 505  $H_{\alpha}$  line profiles and Thomson scattering spectra, *Appl. Phys. Lett.* 107 (2015) 024102 1–4.
- 506 [10] H. Griem, Stark broadening of the hydrogen Balmer- $\alpha$  line in  
507 low and high density plasmas, *Contrib. Plasma Phys.* 40 (2000)  
508 46–56.
- 509 [11] S. Eliezer, A. D. Krumbein, D. Salzmann, Generalized valid-  
510 ity condition for local thermodynamic-equilibrium in a laser-  
511 produced plasma, *J. Phys. D: Appl. Phys.* 11 (1978) 1693–1701.
- 512 [12] G. Cristoforetti, E. Tognoni, L. A. Gizzi, Thermodynamic equi-  
513 librium states in laser-induced plasmas: From the general case to  
514 laser-induced breakdown spectroscopy plasmas, *Spectrochim.*  
515 *Acta Part B: Atom. Spectrosc.* 90 (2013) 1–22.
- 516 [13] M. Boueri, M. Baudelet, J. Yu, X. Mao, S. S. Mao, R. Russo,  
517 Early stage expansion and time-resolved spectral emission of  
518 laser-induced plasma from polymer, *Appl. Surf. Sci.* 255 (2009)  
519 9566–9571.
- 520 [14] Q. Ma, V. Motto-Ros, F. Laye, J. Yu, W. Lei, X. Bai, L. Zheng,  
521 H. Zeng, Ultraviolet versus infrared: Effects of ablation laser  
522 wavelength on the expansion of laser-induced plasma into one-  
523 atmosphere argon gas, *J. Appl. Phys.* 111 (2012) 1–11.
- 524 [15] I. N. Mihailescu, J. Hermann, Laser-plasma interactions, in:  
525 P. Schaaf (Ed.), *Laser Processing of Materials*, Springer, Berlin,  
526 2010, pp. 49–88.
- 527 [16] M. Burger, D. Pantić, Z. Nikolić, S. Djeniže, Shielding effects  
528 in the laser-generated copper plasma under reduced pressures of  
529 He atmosphere, *J. Quant. Spectrosc. Radiat. Transf.* 170 (2016)  
530 19–27.
- 531 [17] L. Mercadier, J. Hermann, C. Grisolia, A. Semerok, Diagnostics  
532 of nonuniform plasmas for elemental analysis via laser-induced  
533 breakdown spectroscopy: demonstration on carbon-based materi-  
534 als, *J. Anal. At. Spectrom.* 28 (2013) 1446–1455.
- 535 [18] J. Hermann, C. Gerhard, E. Axente, C. Dutouquet, Comparative  
536 investigation of laser ablation plumes in air and argon by anal-  
537 ysis of spectral line shapes: Insights on calibration-free laser-  
538 induced breakdown spectroscopy, *Spectrochim. Acta Part B:*  
539 *Atom. Spectrosc.* 100 (2014) 189–196.
- 540 [19] M. S. Dimitrijević, S. Sahal-Bréchet, Stark broadening of neu-  
541 tral calcium spectral lines, *Astron. Astrophys. Supp.* 140 (1999)  
542 191–192.
- 543 [20] J. Chapelle, S. Sahal-Bréchet, Experimental and theoretical  
544 electron impact broadening of some Mg II and Ca II lines of  
545 astrophysical interest, *Astron. Astrophys.* 6 (1970) 415–422.
- 546 [21] J. S. Hildum, J. Cooper, Stark broadening of calcium ion re-  
547 sonance lines, *Phys. Lett.* 36A (1971) 153–155.
- 548 [22] J. Purić, N. Konjević, Stark shifts of some isolated spectral lines  
549 of singly ionized earth alkaline metals, *Z. Phys.* 249 (1972) 440–  
550 444.
- 551 [23] W. W. Jones, A. Sanchez, J. R. Greig, H. R. Griem, Measure-  
552 ment and calculation of the Stark-broadening parameters for the  
553 resonance lines of singly ionized calcium and magnesium, *Phys.*  
554 *Rev. A* 5 (1972) 2318–2328.
- 555 [24] H. Kusch, H. Pritschow, Broadening and shift of calcium lines  
556 by microfields, *Astron. Astrophys.* 4 (1970) 31–35.
- 557 [25] R. Hühn, H. Kusch, Broadening and shift of calcium lines by  
558 van der Waals interaction with argon atoms and by electron im-  
559 pact, *Astron. Astrophys.* 28 (1973) 159–164.
- 560 [26] D. Hadžiomerspahić, M. Platiša, N. Konjević, M. Popović, Stark  
561 broadening and shift of some isolated spectral lines of singly  
562 ionised earth alkaline metals, *Z. Phys.* 262 (1973) 169–179.
- 563 [27] J. F. Baur, J. Cooper, A shock tube study of line broadening  
564 in a temperature range of 6100 to 8300 K, *J. Quant. Spectrosc.*  
565 *Radiat. Transf.* 17 (1977) 311–322.
- 566 [28] C. Fleurier, S. Sahal-Bréchet, J. Chapelle, Stark profiles of some  
567 ion lines of alkaline earth elements, *J. Quant. Spectrosc. Radiat.*  
568 *Transf.* 17 (1977) 595–604.
- 569 [29] C. Goldbach, G. Nollez, P. Plomdeur, J.-P. Zimmermann, Stark-  
570 width measurements of singly ionized calcium resonance lines  
571 in a wall-stabilized arc, *Phys. Rev. A* 28 (1983) 234–237.
- 572 [30] A. Srečković, S. Djeniže, Measured Stark width and shift of  
573 393.367 nm Ca II resonance spectral line, *Bull. Astron. Belgr.*  
574 148 (1993) 7–10.
- 575 [31] J. A. Aguilera, C. Aragón, J. Manrique, Measurement of Stark  
576 widths and shifts of Ca II spectral lines, *MNRAS* 444 (2014)  
577 1854–1858.
- 578 [32] M. S. Dimitrijević, S. Sahal-Bréchet, Stark broadening param-  
579 eter tables for neutral calcium spectral lines, *Serb. Astron. J.* 161  
580 (2000) 39–88.
- 581 [33] M. S. Dimitrijević, S. Sahal-Bréchet, Stark broadening param-  
582 eter tables for Ca II lines of astrophysical interest, *Bull. Astron.*  
583 *Belgr.* 145 (1992) 81–99.
- 584 [34] M. S. Dimitrijević, S. Sahal-Bréchet, Stark broadening of Ca  
585 II spectral lines, *J. Quant. Spectrosc. Radiat. Transf.* 49 (1993)  
586 157–164.
- 587 [35] I. Tapalaga, I. P. Dojčinović, M. K. Milosavljević, J. Purić, Stark  
588 width regularities within neutral calcium spectral series, *Publ.*  
589 *Astron. Soc. Aust.* 29 (2012) 20–28.
- 590 [36] M. Cirisan, M. Cvejić, M. Gavrilović, S. Jovicević, N. Konjević,  
591 J. Hermann, Stark broadening measurement of Al II lines in a  
592 laser-induced plasma, *J. Quant. Spectrosc. Radiat. Transf.* 133  
593 (2014) 652–662.
- 594 [37] C. Gerhard, J. Hermann, L. Mercadier, L. Loewenthal, E. Ax-  
595 ente, C. Luculescu, T. Sarnet, M. Sentis, W. Viöl, Quantitative  
596 analyses of glass via laser-induced breakdown spectroscopy in  
597 argon, *Spectrochim. Acta Part B: Atom. Spectrosc.* 101 (2014)  
598 32–45.
- 599 [38] X. Z. Zhao, L. J. Shen, T. X. Lu, K. Niemax, Spatial distri-  
600 butions of electron-density in microplasmas produced by laser  
601 ablation of solids, *Appl. Phys. B: Photophys. Laser Chem.* 55  
602 (1992) 327–330.
- 603 [39] E. Tognoni, V. Palleschi, M. Corsi, G. Cristoforetti,  
604 N. Omenetto, I. Gornushkin, B. W. Smith, J. D. Winefordner,  
605 From sample to signal in laser-induced breakdown spectroscopy:  
606 a complex route to quantitative analysis, in: A. W. Miziolek,  
607 V. Palleschi, I. Schechter (Eds.), *Laser-induced break-*  
608 *down spectroscopy*, Cambridge University, Berlin, 2006, pp.  
609 122–194.
- 610 [40] M. A. Gigosos, M. A. Gonzalez, V. Cardenoso, Computer sim-  
611 ulated Balmer-alpha, -beta, and -gamma Stark line profiles for  
612 non-equilibrium plasma diagnostics, *Spectrochim. Acta Part B:*  
613 *Atom. Spectrosc.* 58 (2003) 1489–1504.
- 614 [41] A. D. Giacomo, M. Dell’Aglio, R. Gaudiuso, G. Cristoforetti,  
615 S. Legnaioli, V. Palleschi, E. Tognoni, Spatial distribution of  
616 hydrogen and other emitters in aluminum laser-induced plasma  
617 in air and consequences on spatially integrated laser-induced  
618 breakdown spectroscopy measurements, *Spectrochim. Acta Part*  
619 *B: Atom. Spectrosc.* 63 (9) (2008) 980–987.
- 620 [42] J. Hermann, A. Lorusso, A. Perrone, F. Strafella, C. Dutouquet,  
621 B. Torralba, Simulation of emission spectra from nonuniform  
622 reactive laser-induced plasmas, *Phys. Rev. E* 92 (2015) 1–15.
- 623 [43] A. Radzig, B. Smirnov, *Reference Data on Atoms, Molecules*  
624 *and Ions*, Springer, Berlin, 1985.
- 625 [44] A. Kramida, Y. Ralchenko, J. Reader, Nist Atomic Spectra  
626 Database, National Institute of Standards and Technology,  
627 Gaithersburg, MD (2016).  
628 URL <http://physics.nist.gov/asd>
- 629 [45] M. Burger, M. Skočić, M. Ljubisavljević, Z. Nikolić, S. Djeniže,  
630 Spectroscopic study of the laser-induced indium plasma, *Eur.*  
631 *Phys. J. D* 68 (2014) 223:1–8.
- 632 [46] D. Bulajic, M. Corsi, G. Cristoforetti, S. Legnaioli, V. Palleschi,  
633 A. Salvetti, E. Tognoni, A procedure for correcting self-  
634

- 635 absorption in calibration free-laser induced breakdown spec-  
636 troscopy, *Spectrochim. Acta Part B: Atom. Spectrosc.* 57 (2002)  
637 339–353.
- 638 [47] R. McWhirter, Ch. 5, in: R. H. Huddleston (Ed.), *Plasma Diag-*  
639 *nostic Techniques*, Academic, New York, 1965, pp. 201 – 264.
- 640 [48] N. Konjević, M. Ivković, N. Sakan, Hydrogen Balmer lines for  
641 low electron density plasma diagnostics, *Spectrochim. Acta Part*  
642 *B: Atom. Spectrosc.* 76 (2012) 16–26.
- 643 [49] S. Djeniže, A. Srečković, S. Bukvić, The C I 247.8561 nm reso-  
644 nance line stark broadening parameters, *Z. Naturfors. Sect. A-J.*  
645 *Phys. Sci.* 61 (2006) 91–94.
- 646 [50] M. Skočić, M. Burger, Z. Nikolić, S. Bukvić, S. Djeniže, Stark  
647 broadening in the laser-induced Cu I and Cu II spectra, *J. Phys.*  
648 *B* 46 (2013) 185701:1–6.
- 649 [51] S. Djeniže, S. Bukvić, A. Srečković, Stark broadening and tran-  
650 sition probability ratios in the Mg I spectrum, *Astron. Astro-*  
651 *phys.* 425 (2004) 361–365.
- 652 [52] S. Bukvić, A. Srečković, S. Djeniže, Mg II h and k lines Stark  
653 parameters, *New Astron.* 9 (2004) 629–633.
- 654 [53] S. Djeniže, S. Bukvić, A. Srečković, M. Platiša, Mg II spectral  
655 line broadening in helium, oxygen and argon-helium plasmas,  
656 *Astron. Astrophys.* 424 (2004) 561–564.
- 657 [54] S. Bukvić, S. Djeniže, A. Srečković, Line broadening in the Si  
658 I, Si II, Si III, and Si IV spectra in the helium plasma, *Astron.*  
659 *Astrophys.* 508 (2009) 491–500.
- 660 [55] C. Aragón, J. Aguilera, J. Manrique, Measurement of Stark  
661 broadening parameters of Fe II and Ni II spectral lines by laser  
662 induced breakdown spectroscopy using fused glass samples, *J.*  
663 *Quant. Spectrosc. Radiat. Transf.* 134 (2014) 39–45.
- 664 [56] C. Aragón, P. Vega, J. Aguilera, Stark width measurements of  
665 Fe II lines with wavelengths in the range 260-300 nm, *J. Phys.*  
666 *B* 44 (2011) 55002:1–7.